



Improving hierarchical porous structure of carbon aerogels for more efficient ion transport for supercapacitors with commercial level mass loading

Dong Wang ^a, Wei Fan ^{a, **}, Shijia Yuan ^a, Tianxi Liu ^{a, b, c, *}

^a State Key Laboratory for Modification of Chemical Fibers and Polymer Materials, College of Materials Science and Engineering, Donghua University, 2999 North Renmin Road, Shanghai, 201620, PR China

^b Key Laboratory of Synthetic and Biological Colloids, Ministry of Education, School of Chemical and Material Engineering, Jiangnan University, Wuxi, 214122, PR China

^c Key Laboratory of Materials Processing and Mold (Zhengzhou University), Ministry of Education, Zhengzhou, 450002, PR China



ARTICLE INFO

Article history:

Received 22 July 2019

Received in revised form

26 August 2019

Accepted 1 September 2019

Available online 5 September 2019

Keywords:

Carbon aerogel

Heteroatom-doping

Hierarchical pore

Supercapacitor

ABSTRACT

Designing porous structure and surface properties of carbon electrodes is the key premise for efficient electron/ion transfer, which is crucial for improving electrochemical performance of supercapacitors in practical applications. Herein, N-doped activated carbon aerogel (NACA) with hierarchical porous structure and N, O-rich functionalities has been prepared from polyimide gel by activation and carbonization process. The NACA exhibits a high surface area of $1410 \text{ m}^2 \text{ g}^{-1}$ with hierarchical porous structures, with both high micropore volume (0.481 cc g^{-1}) and mesopore volume (0.566 cc g^{-1}) as well as high heteroatom content, which is favorable for charge storage, ion transfer and electrolyte penetration. As a result, the NACA2-11 can deliver a high capacitance of 386 F g^{-1} at 1 A g^{-1} in a three-electrode system and outstanding rate performance with the capacitance retaining 150 F g^{-1} at 100 A g^{-1} in aqueous electrolyte. Furthermore, the practical two-electrode device exhibits a high areal specific capacitance of 1584 mF cm^{-2} under the commercial level mass loading of 10 mg cm^{-2} , and it stays a good cycling stability of 93% capacitance retention after 10000 cycles at 5 A g^{-1} . This study paves the way for improving electrochemical performance of carbon-based supercapacitor under high mass loadings.

© 2019 Elsevier Ltd. All rights reserved.

1. Introduction

Supercapacitors are promising electrochemical energy storage units due to their high power density, long cyclic life, and fast charge-discharge rates [1–3]. Although there is a tremendous interest in developing pseudocapacitive materials because of their high energy density [4,5], the practical application of pseudocapacitive materials is still restricted due to the poor cycling stability [6]. Currently, carbon-based electrode materials based on electrical double layer (EDL) capacitance is still the most widely applied for supercapacitors [7–9]. However, the energy density of

supercapacitors based on carbon electrode is still unsatisfied. Although some previous works have reported the energy density of $50\text{--}100 \text{ Wh kg}^{-1}$, the mass loadings of these electrodes are only $0.5\text{--}1 \text{ mg cm}^{-2}$, much lower than that ($\sim 10 \text{ mg cm}^{-2}$) required for commercial supercapacitors [10,11]. Moreover, excellent rate performance is preferred for supercapacitors for practical use under high charging densities [12]. Although some studies have reported a high specific capacitance of $300\text{--}400 \text{ F g}^{-1}$ for carbon electrodes, these values are normally obtained under small current densities ($<1 \text{ A g}^{-1}$), which is not suitable for practical use for fast charging [13–15]. Therefore, it is highly desirable to explore new electrode materials that have high energy density and good rate performance at high mass loading while remaining good cycling stability [16,17]. However, higher mass loading would increase the thickness of the electrode, which leads to longer charge transport distance and prolonged ion diffusion pathway, resulting in inferior rate performance of supercapacitors [18]. To address these challenges,

* Corresponding author. Key Laboratory of Materials Processing and Mold (Zhengzhou University), Ministry of Education, Zhengzhou, 450002, PR China.

** Corresponding author.

E-mail addresses: weifan@dhu.edu.cn (W. Fan), txliu@dhu.edu.cn, txliu@fudan.edu.cn (T. Liu).

designing new carbon electrode materials with large ion-accessible surface area and efficient electron/ion transport pathways is urgently needed [19,20].

Porous carbon materials are proverbially used as electrode materials for supercapacitors [21–23]. The pore size distribution, specific surface area and surface properties of carbon electrode have a significant influence on the electrochemical performance of supercapacitors. High surface area of carbon materials benefits the formation of electrical double layer, while pore size distribution determines the ion diffusion pathways [24]. Some researchers have reported that pore size less than 1 nm that ideally matches the ions size of electrolyte can effectively store charge, thus improving the EDL capacitance. However, vast microporous network leads to an unfavorable ion diffusion process especially at high current densities. The sluggish ion diffusion into micropores is unable to keep pace with the fast charging and discharging rate, thus resulting in an inferior rate performance. The presence of mesopores could accelerate transport of electrolyte ions for good dynamic charge propagation, while macropores serve as the ion buffering reservoirs which can further decrease the ion transfer distance [25]. Therefore, hierarchical pores are highly desirable for carbon electrodes for both improved charge storage and ion diffusion, which is significant for realizing a high capacitance at higher current densities and mass loadings.

Carbon aerogels are considered as promising candidates for supercapacitor electrode because of their high surface area, high porosity and good electrical conductivity. Conventionally, carbon aerogels are derived from the pyrolysis process of an organic aerogel, typically resorcinol-formaldehyde aerogel [26]. Although there is an emerging interest in developing new category of carbon aerogels such as graphene or carbon nanotube aerogels, their practical application in supercapacitors is still restricted due to complex synthesis process and costly raw materials. More importantly, the pore size of graphene or carbon nanotube aerogels is mainly in the meso- and macroporous range, and the surface area is normally below $500 \text{ m}^2 \text{ g}^{-1}$, which is not favorable for charge storage. In fact, carbon aerogels derived from phenol-based organic gels with tunable porous structure are more suitable for practical application in supercapacitors. Besides, carbon aerogels derived from organic gels usually contain certain heteroatoms, which can introduce additional pseudo-capacitance and improve wettability. Typical fabrication procedure including sol-gel transition, drying and carbonization is needed for fabrication of RF-based carbon aerogels. Besides, additional activation agents (e.g. CO_2 , KOH, K_2CO_3 , ZnCl_2) are commonly applied to achieve high surface area for carbon aerogels [27,28]. However, such prepared carbon aerogels usually have a large number of ultra-micropores (pore diameter $< 0.7 \text{ nm}$), which fails in the formation of electrical double-layer and increase ion diffusion resistance, leading to poor rate performance [29–32]. To facilitate ion diffusion and improve the dynamic charge propagation, various efforts have been made to increase mesoporous volume of carbon aerogels by utilizing templates, such as poly(propylene glycol)-block-poly(ethylene glycol)-block-poly(propylene glycol) (PPO-PEO-PPO) block copolymer [33] and inorganic pre-hydrolyzed tetraethyl orthosilicate [34]. Unfortunately, these methods include tedious fabrication process and the precise control over the microporosity and mesoporosity of carbon aerogels still lacks. Therefore, the economical fabrication of carbon aerogels with an integration of large surface area, hierarchical porous structure and surface functionalities remains challenging.

Herein, N-doped activated carbon aerogel (NACA) with hierarchical porous structure has been prepared from nitrogen-rich polyimide gel by activation and carbonization process. The NACA exhibits a high surface area of $1410 \text{ m}^2 \text{ g}^{-1}$ with multi-scaled porous structures, in which micropores and mesopores can be

easily controlled by tuning activating agent (KOH) and nitrogen sources (urea). The optimized NACA exhibits both high micropore volume (0.481 cc g^{-1}) and mesopore volume (0.566 cc g^{-1}) as well as high heteroatom content, which favors charge storage, ion diffusion and electrolyte penetration. As a result, the as-prepared NACA exhibits a high capacitance of 386 F g^{-1} at 1 A g^{-1} and outstanding rate performance with the capacitance still retains 150 F g^{-1} at 100 A g^{-1} in aqueous electrolyte. Due to the fast ion diffusion and reduced charge transfer resistance, the NACA manifests good capacitive performance with areal specific capacitance of 1584 mF cm^{-2} when the mass loading increased to commercial level of 10 mg cm^{-2} . Therefore, such all-carbon electrode with high capacitance and good rate performance at the high mass loading provides alternative for development of commercial carbon-based electrodes.

2. Experimental section

2.1. Preparation of N-doped activated carbon aerogel (NACA)

The precursor of polyimide, polyamide acid (PAA), was synthesized by a polymerization process according to our previous report [25]. Typically, 2 g PAA was immersed in 20 mL graphene oxide (GO) solution (8 mg ml^{-1}), and 1 g triethylamine was dropwise added until it dissolved completely. KOH was subsequently added with different proportions to PAA (PAA: KOH = 2:1; 3:1) into the above solution to obtain the PAA/GO/KOH hydrogel. Then, the PAA/GO/KOH hydrogels were freeze-dried in liquid nitrogen and transferred into the freezing dryer to obtain PAA/GO/KOH aerogels. The aerogels were placed in the tube furnace for imidization process at 300°C for 1 h, and activation at 750°C for 1.5 h in nitrogen atmosphere. Finally, the obtained samples were mixed with urea and carbonized in tube furnace at 1000°C in nitrogen atmosphere for 2 h. The resultant samples are named as NACAx-y, in which x stands for the ratio of PAA to KOH (2:1; 3:1; 4:1) and y stands for the ratio of carbon aerogel to urea (2:1, 1:1, 1:2). For comparison, carbon aerogels without adding KOH or urea were prepared by the same procedure, which were named as CA or ACA, respectively.

2.2. Characterization

The morphologies of the CA, ACAs and NACAs were observed using field-emission scanning electron microscopy (FESEM, S-4800, Hitachi) and transmission electron microscopy (TEM, JEM-2100, JEOL) with an EDS detector. Quadrasorb adsorption instrument (Quantachrome Instruments) was used for nitrogen sorption/desorption measurements. The pore size distributions were calculated from nitrogen sorption data using the nonlocal density functional theory (NLDFT) equilibrium model method. Raman spectra were tested by using an inVia Reflex Raman Spectrometer (inVia-Reflex, Renishaw) with a 532 nm laser diode as the excitation source. X-ray photoelectron spectroscopy (XPS) was characterized using a spectrometer (Escalab 250Xi) with Al K α X-ray radiation.

2.3. Electrochemical measurements

The electrochemical measurements were conducted using the electrochemical working station (CHI660E, Shanghai, China). A homogeneous slurry of working electrodes was prepared by mixing active materials, acetylene black as conductive agent and polyvinylidene fluoride (PVDF) as binder in a weight ratio of 8:1:1 with N-methyl-2-pyrrolidone (NMP) applied as solvent, and then the slurry (about 1 mg) was coated onto a graphite paper ($1 \times 1 \text{ cm}^2$) as the current collector. Finally, the electrodes were prepared after

drying process at 80 °C overnight. For three-electrode measurements, platinum wire was used as the counter electrode and Ag/AgCl as the reference electrode. For two-electrode system, two pieces of graphite paper ($1 \times 1 \text{ cm}^2$) with electrode materials (1 mg, 2 mg, 5 mg, 10 mg) separated by a cellulose separator were tested in 1 M H₂SO₄. The electrochemical performance of electrodes was evaluated by cyclic voltammetry (CV) at various scan rates from 10 to 200 mV s⁻¹ and galvanostatic charge-discharge measurements at different current density from 1 A g⁻¹ to 100 A g⁻¹. Electrochemical impedance spectroscopy (EIS) was conducted in the frequency range from 100 kHz to 10 mHz with an AC voltage amplitude of 5 mV. The charge transfer impedance (R_{ct}) is calculated by the software ZsimDemo.

In the two-electrode system, the gravimetric specific capacitance (C_g) was calculated according to the following equation:

$$C_g = \frac{2I\Delta t}{m\Delta V}$$

where I, Δt , ΔV , and m are the current (A), the discharge time (s), the voltage change (V), and the total mass of active materials (g), respectively.

The areal specific capacitances (C_a) were evaluated according to the following equation:

$$C_a = C_g M_l$$

where C_g (F g⁻¹) is gravimetric specific capacitance of electrode, M_l (g cm⁻²) is the areal density of electrode material.

The areal energy density (E_a) and the areal power density (P_a) based on the symmetric two-electrode supercapacitor were calculated as the following two equations:

$$E_a = \frac{1}{2} C_a \times V^2 \times \frac{1}{2} \times \frac{1}{3.6}$$

$$P_a = \frac{3600 E_a}{t}$$

where C_a is the areal capacitance of the symmetric supercapacitor device, V is the operation potential window, and t is the discharge time.

3. Result and discussion

3.1. Morphologies and characterization of NACA

N-doped activated carbon aerogels (NACA) with hierarchical porous structure have been fabricated by employing polyimide as carbon precursor with KOH activation and N-doping. Polyamide acid (PAA) oligomer, graphene oxide (GO) and KOH were first mixed to form a hydrogel followed by freeze-drying to obtain PAA/GO/KOH aerogel. The aerogel was activated by KOH at 750 °C and subsequently carbonized with urea to obtain the final NACA. The fabricating process is illustrated in Fig. 1 and digital photos of CA, ACA2, NACA2-11 have been provided in Fig. S1. All the samples show the bulk monolith morphologies, indicating the formation of aerogel structures. During the thermal treatment, polyimide turns into carbon, KOH activates carbon to form micropores, and urea further accelerates increase of mesopore volume as well as introduces nitrogen. The resultant NACA exhibits a multi-scale porous structure due to the KOH activation and ion diffusion as electrodes.

The morphologies and pore structures of CA, ACA2, NACA2-11 are characterized by SEM. As shown in Fig. 2a, CA exhibits a porous morphology, which has a macropore size about 2–3 μm and solid pore walls (Fig. S2). These micron-sized cavities take shape during the freeze-drying process, caused by the sublimation of water in the hydrogel. After activation by KOH, the pores of ACA2 become much smaller, with pore size in the range of several hundred nanometers (Fig. 2b, Fig. S3) [35]. With N-doping, NACA2-11 exhibits hierarchical porous structure (Fig. 2c). The multi-scale porous structure is further confirmed by TEM observation in Fig. 2d. Enlarged TEM images of NACA2-11 show that mesopores are uniformly dispersed on the wall of aerogel (Fig. 2e). Fig. 2f reveals the coexistence of graphene phase (red circles) and amorphous carbon phase (blue circles), providing an evidence for the formation of defect caused by the final carbonization process. The EDS elemental mappings of NACA2-11 show uniform distributions of nitrogen and oxygen elements in the carbon aerogel framework (Fig. 2g), suggesting the successful N-doping and O-doping of carbon aerogel.

The N₂ adsorption-desorption isotherms of CA, ACA2, NACA2-11 in Fig. 3a show that all the samples are classified as type IV curves, indicating the presence of mesopores and macropores. The N₂ adsorption amount of NACA2-11 exhibits a faster rise under lower pressure ($P/P_0 < 0.01$) than the other two samples (as shown by

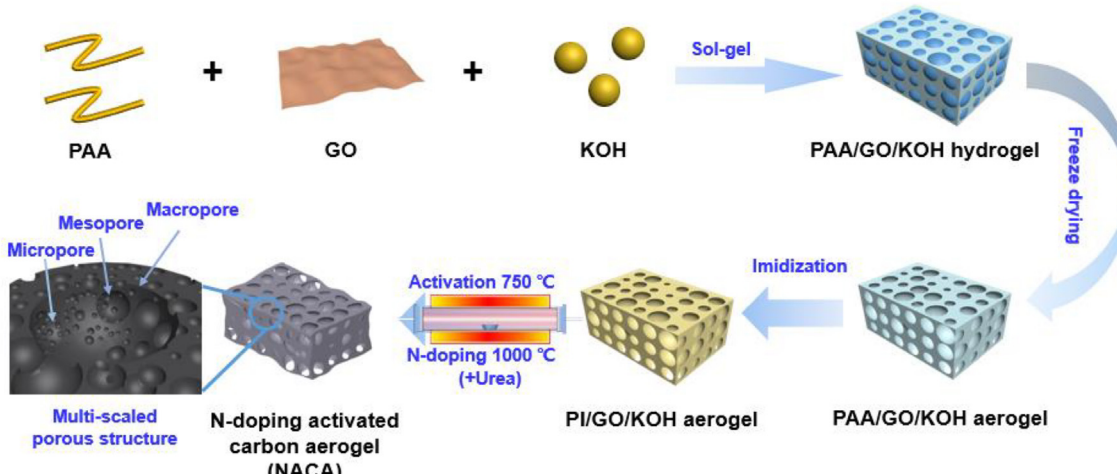


Fig. 1. Schematic illustration of the fabrication process of NACA.

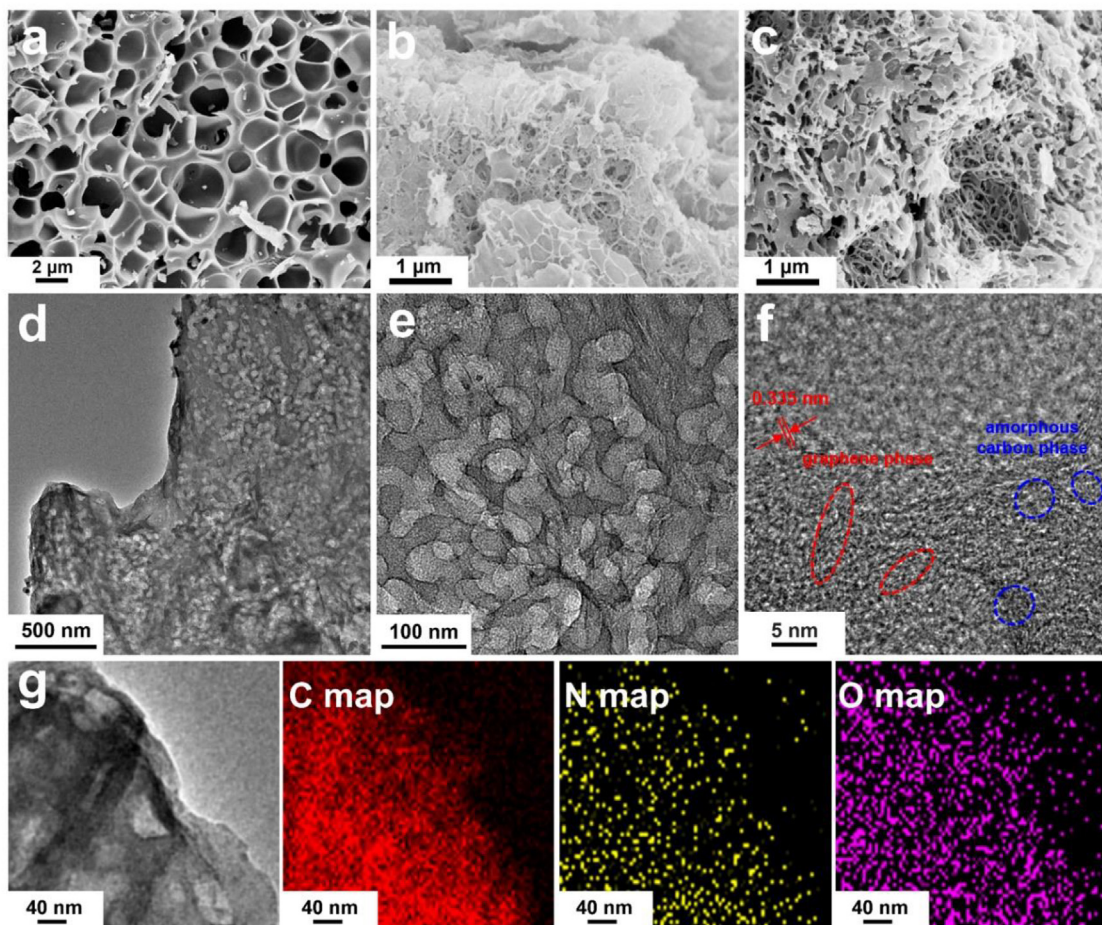


Fig. 2. SEM images of (a) CA, (b) ACA2, (c) NACA2-11. (d, e, f) TEM images of the NACA2-11 and (g) corresponding EDS elemental mapping images of carbon, nitrogen and oxygen elements.

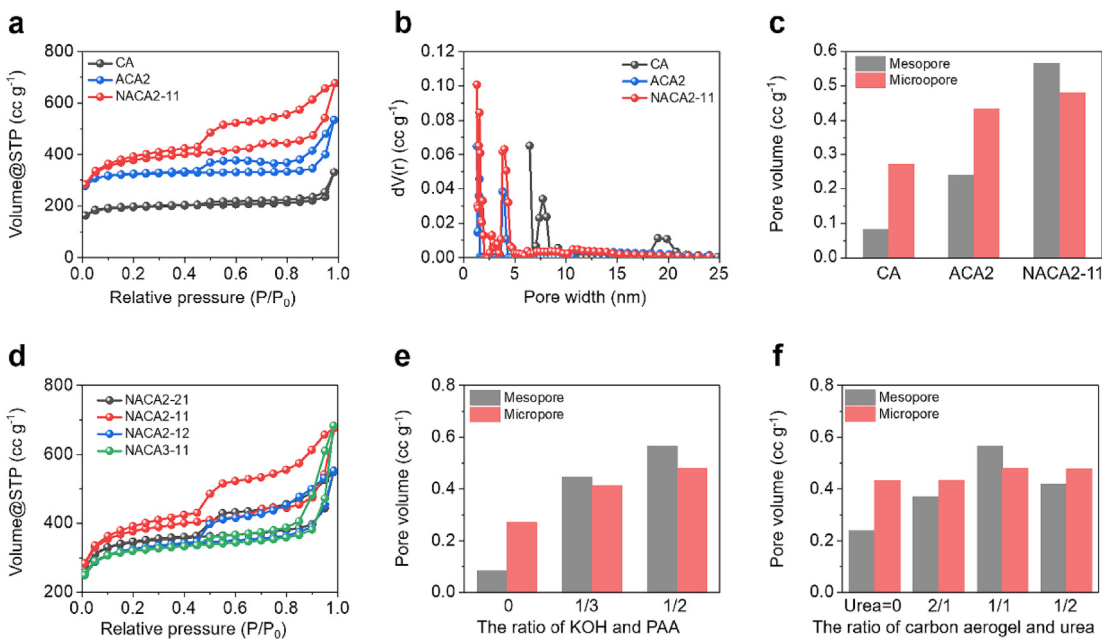


Fig. 3. (a) N₂ adsorption-desorption isotherms and (b) pore-size distribution curves of CA, ACA2, NACA2-11. (c) The mesopore volumes and micropore volumes of CA, ACA2, NACA2-11. (d) N₂ adsorption-desorption isotherms of different samples. The mesopore volumes and micropore volumes of different samples with (e) different contents of KOH and (f) different contents of urea.

Table 1

Physical properties and specific capacitance of NACAs.

Samples	BET			XPS			Raman	Capacitance
	Surface Area ($\text{m}^2 \text{ g}^{-1}$)	Mesopore Volume (cc g^{-1})	Micropore Volume (cc g^{-1})	C (at %)	N (at %)	O (at %)	I_D/I_G	$C (\text{F g}^{-1})$
CA	635	0.083	0.271	94.2	1.0	4.8	0.89	193
ACA2	1096	0.240	0.433	90.6	1.8	7.6	0.96	339
NACA2-21	1216	0.421	0.435	94.6	2.0	3.4	1.03	367
NACA2-11	1410	0.566	0.481	89.6	3.9	6.5	1.19	386
NACA2-12	1305	0.372	0.478	93.8	2.4	3.8	1.03	325
NACA3-11	983	0.447	0.415	91.0	3.3	5.7	0.96	377

amplified curves in Fig. S4), which indicates the existence of significant amount of micropores. Moreover, the hysteresis loop of NACA2-11 under relatively high pressure ($0.4 \leq P/P_0 < 0.99$) is more obvious than the other samples caused by capillary condensation in the fissure-shaped mesopores, demonstrating that activation and following N-doping accelerate the formation of hierarchical porous structures [36–39]. As a result, NACA2-11 has a large surface area of $1410 \text{ m}^2 \text{ g}^{-1}$, much larger than that of CA ($635 \text{ m}^2 \text{ g}^{-1}$) and ACA2 ($1096 \text{ m}^2 \text{ g}^{-1}$) (Table 1). The pore-size distribution curves of CA, ACA2, NACA2-11 are shown in Fig. 3b and the corresponding pore volume are displayed in Fig. 3c. The pore sizes of CA are mainly in the mesoporous range while ACA2 and NACA2-11 have a large portion of micropores in addition to mesopores. The activation procedure makes KOH react with carbon skeleton, which produces plenty of gas such as hydrogen, carbon dioxide and carbon monoxide, causing the tapping effect in the inner wall. This reaction significantly increases the micropore volume, from 0.271 cc g^{-1} of CA to 0.433 cc g^{-1} of ACA2-1000, and the mesopore volume, from 0.083 cc g^{-1} to 0.240 cc g^{-1} (Fig. 3c and Table 1). More importantly, the micropore size of NACA2-11 is centered in 1.5 nm, which matches with the size of electrolyte ions that can effectively store charges. After N-doping procedure, mesopore volume of NACA2-11 (0.566 cc g^{-1}) becomes about twice that of ACA2 while micropore volume just has a negligible rise. The nitrogen source can decompose into much compounds including carbon, nitrogen, hydrogen and some gases that can further sculpture carbon matrix for more mesopores [40].

The detailed pore formation mechanism is further examined by varying the dosage of KOH and urea, and the resultant samples are named as NACAx-y, in which x stands for the ratio of PAA to KOH and y stands for the ratio of carbon aerogel to urea. The N_2 adsorption-desorption isotherms and pore-size distribution curves of NACAx-y are shown in Fig. 3d and Fig. S5, and corresponding pore volume are summarized in Fig. 3e and f. As shown in Fig. 3e, by increasing KOH amount, both micropore and mesopore volume increase for NACA2-11 compared with NACA3-11 and CA. However, further increasing the dosage of KOH will affect the formability of the aerogel since the over consumption of carbon during activation process, thus contributing to the collapse of the monolith aerogel structure. As demonstrated in Fig. 3f, the urea amount has a great influence on the mesopore volume of NACAx-y while the micropore volume remains almost the same. In the high temperature process, urea can decompose into small molecular gas such NH_3 and CO_2 , which can make some mesopores easily during the gas overflowing process [41]. NACA2-11 with the ratio of urea to carbon aerogel of 1:1 exhibits the optimized porous structure with both high micropore volume (0.481 cc g^{-1}) and mesopore volume (0.566 cc g^{-1}). Therefore, NACA2-11 exhibits both high micropore and mesopore volume due to the synergistic function of urea and KOH, which benefits the charge storage and ion diffusion respectively as electrode materials for supercapacitors.

The XPS spectra of CA, ACA2, NACA2-11 are shown in Fig. 4a. Three main characteristic peaks are observed at 285.0 eV, 400.1 eV,

531.0 eV, which correspond to C 1s, N 1s, and O 1s, respectively. As shown in Fig. 4b, ACA2 and NACA2-11 show higher oxygen content than CA as KOH activation process increases the oxidation degree of carbon aerogel. The high-resolution O 1s spectrum and C 1s spectrum also confirm the existence of oxygen-containing functionality on carbon materials (Fig. S6). It is reported that those oxygen functional groups can improve the wettability of porous carbon material while it enables electrolyte permeate into the porous structure easier. The surface $-\text{OH}$ or $-\text{COOH}$ groups on porous carbon materials can improve hydrophilicity of porous carbon surface and play a role as active centers for water or electrolyte adsorption, which contributes to much better electrochemical performance [42,43]. The nitrogen content calculated from XPS results are 1.0, 1.8, 3.9 at% for CA, ACA2, NACA2-11, respectively. The higher N content of NACA2-11 indicates the effective N-doping during the carbonization with urea. As displayed in the high-resolution N 1s spectrum (Fig. 4c), the deconvolution suggests four components, including pyrrolic N (N-5, 399.1 eV), pyridinic N (N-6, 398.2 eV), and pyridine-N-oxide (N-X, 403.2 eV), and graphitic N (N-Q, 401.2 eV). Nitrogen atoms contribute to fast electrolyte ion transport and facilitate electron transfer in the carbon electrode, contributing to improved electrochemical performance of supercapacitors [44,45]. Heteroatom doping would induce certain degree of disorder of carbon materials which can be characterized by Raman spectroscopy (Fig. 4d). The peaks located at 1350 and 1596 cm^{-1} correspond to the typical D band and G band of carbon materials, respectively. The ratio of the relative intensity of D band and G band (I_D/I_G) is in direct proportion to the disorder of carbon nanomaterials. The value of I_D/I_G of NACA2-11 is 1.19, higher than that of ACA2 (0.96) and CA (0.89). The increased I_D/I_G value indicates higher disorder degree of carbon nanomaterials, which may be due to that oxygen and nitrogen functional groups are introduced into nanostructures during the activation and N-doping process.

3.2. Electrochemical performance of NACA

Taking the hierarchical porous structures and improved surface functionalities into consideration, the N-doped activated carbon aerogels are promising electrode materials for supercapacitors. Electrochemical performance of CA, ACA2, NACA2-11 are first investigated with a three-electrode system in 1 M H_2SO_4 . As shown in Fig. 5a, all the CV curves exhibit quasi-rectangular shapes with some fluctuation, indicating that these carbon aerogels have good EDL capacitive properties besides a small pseudo-capacitance. It is easy to observe that NACA2-11 exhibits the largest CV area, indicating its larger capacitance compared to CA and ACA2. The higher capacitance of NACA2-11 reveals the importance of hierarchical porous structures for double layer capacitor and multiple electron structures for pseudocapacitance, resulting from the redox reactions of oxygen and nitrogen functionalities. Meanwhile, the isosceles triangular-shaped galvanostatic charge and discharge (GCD) profiles collected at the current density of 1 A g^{-1} indicate

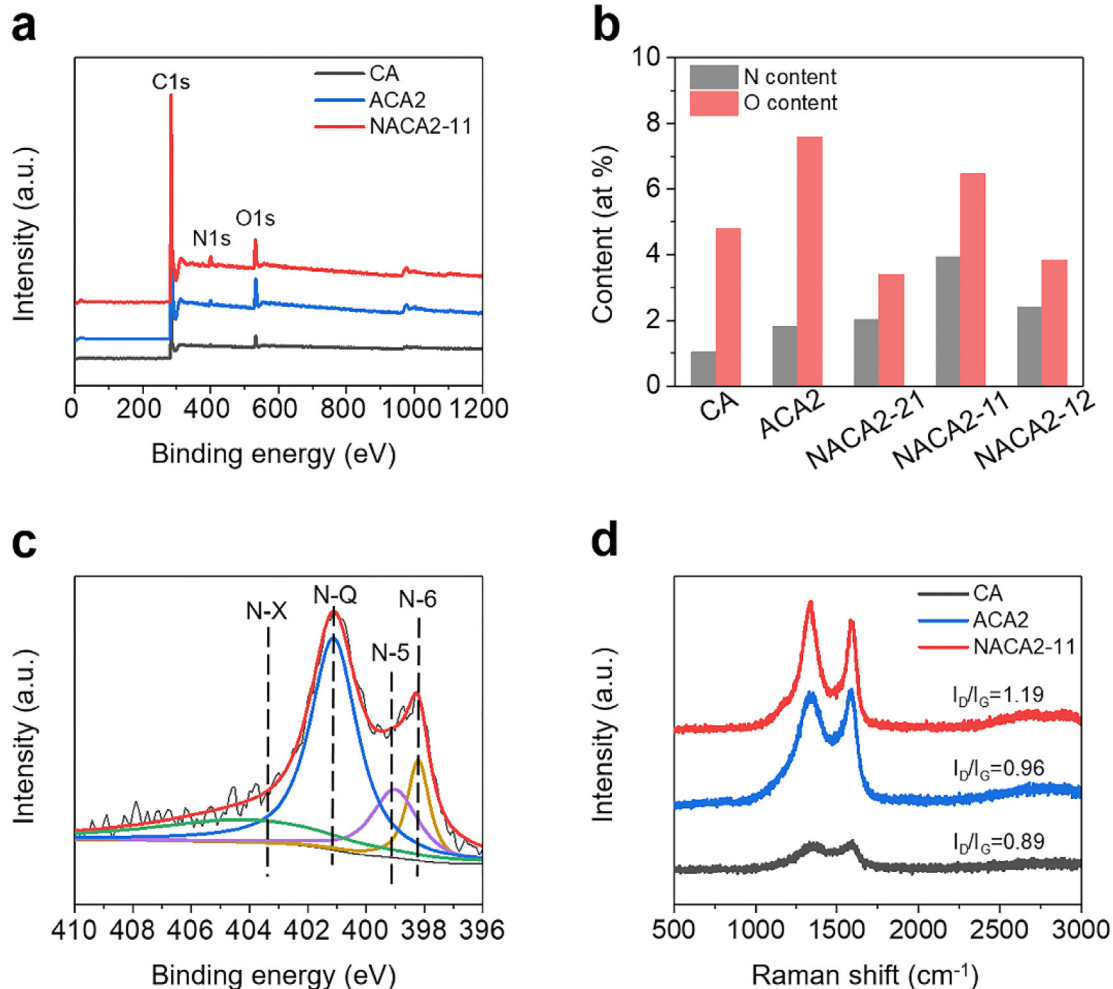


Fig. 4. (a) XPS survey scans of CA, ACA2, NACA2-11. (b) The N content and O content of CA, ACA2, NACAx-y. (c) High-resolution N 1s spectrum of NACA2-11. (d) Raman spectra of CA, ACA2, NACA2-11.

that NACA2-11 has almost ideal capacitive behavior and it yields an excellent gravimetric capacitance of 386 F g^{-1} (Fig. 5b). The IR drops in GCD profiles are negligible, demonstrating good conductivity of NACA2-11.

The capacitance of NACAx-y prepared with different contents of activating agents and urea is also compared as shown in Figs. S7–S8 and summarized in Fig. 5c. NACA2-11 shows higher capacitance compared with NACA3-11, which can be ascribed to the increased micropore and mesopore volume by increasing KOH amount as indicated by BET data (Fig. 3e). As for NACAx-y prepared with various ratios of carbon aerogel to urea, NACA2-11 exhibits the highest capacitance among the three samples due to its optimized porous structure with both high micropore and mesopore volume. Therefore, the specific capacitance of carbon aerogels is highly related to their surface area and porous structures. Micropores contributes to better charge storage capability resulting in higher capacitance, while mesopores facilitate the fast ion diffusion resulting in better rate performance. The good rate performance of NACA2-11 can be indicated by CV curves obtained at different scan rates, which keeps the quasi-rectangular shape well even at a high scan rate of 100 mV s^{-1} (Fig. S9). The specific capacitances of CA, ACA2, NACA2-11 at current densities ranging from 1 to 100 A g^{-1} are demonstrated in Fig. 5d. It is worthy to note that the specific capacitance of NACA2-11 is up to 234 F g^{-1} at 20 A g^{-1} , which keeps 64% retention of that at 1 A g^{-1} . More significantly, the electrode

achieves a higher specific capacitance of 150 F g^{-1} at 100 A g^{-1} , indicating its good rate capability at high charging rates. Such a combination of high capacitance and excellent rate performance of NACA2-11 is originated from the high level of microporosity and mesoporosity, which facilitates fast ion diffusion, especially at higher charging rates.

Nyquist plots of CA, ACA2, NACA2-11 are shown in Fig. 5e, and the inset shows a magnified view in the high-frequency region. In the low-frequency region, NACA2-11 exhibits a more vertical line much closer to vertical axis than those of the other two samples, represents a good capacitive behavior. The intersection at the X-axis in the high-frequency range represents solution resistance. Both ACA2 and NACA2-11 show much lower solution resistance than CA, demonstrating the easier electrolyte accessibilities because of hierarchical porous structure and better wettability because of heteroatom doping. Bode plot is an intuitionistic exhibition for hierarchical porous materials. Firstly, as shown in Fig. 5f, the phase angles of three samples are approximate to -90° at low frequencies of 10^{-2} Hz in the Bode plots, demonstrating a desired capacitive behavior. Secondly, the frequency at the phase angle of 45° is named characteristic frequency, standing for the point where the capacitive impedances is equal to resistance impedances, with the corresponding time constant $\tau_0 (1/f_0)$ that is the shortest time required for discharging all the energy from the device [46]. As shown in Fig. 5f, the τ_0 calculated from Bode plots of CA, ACA2 and

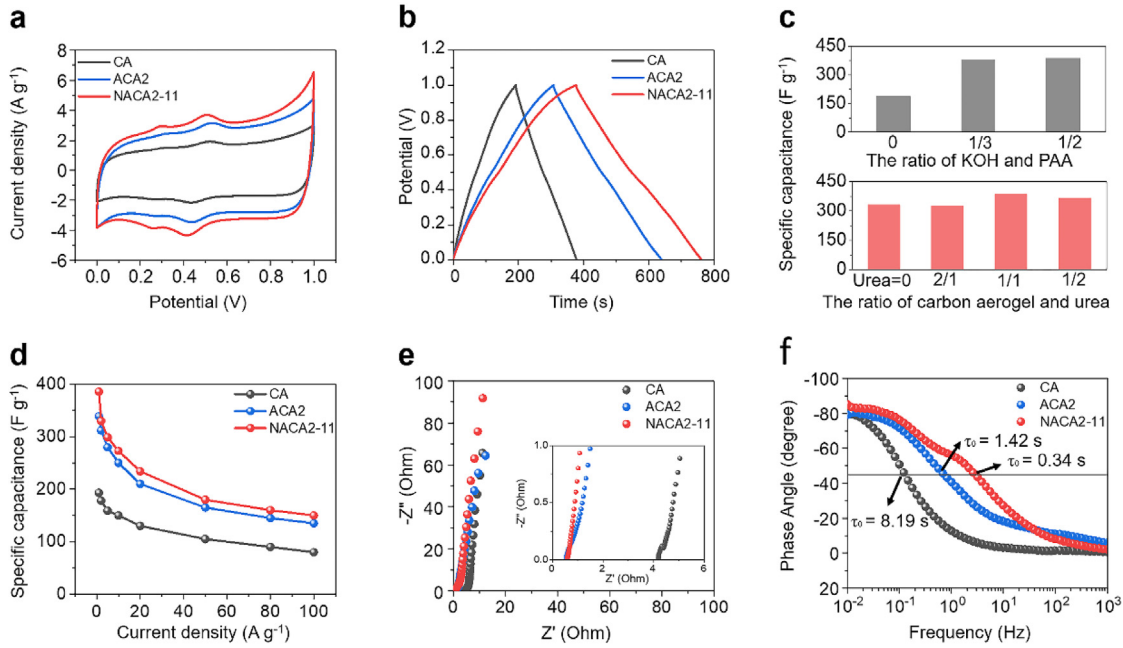


Fig. 5. Electrochemical performance of NACAs measured with a three-electrode system in 1 M H_2SO_4 . (a) CV curves at different scan rates and (b) GCD curves at a current density of 1 A g^{-1} . (c) The specific capacitance of NACAx-y prepared with different contents of KOH and urea. (d) Rate performance and (e) Nyquist plots of CA, ACA2, NACA2-11. (f) Bode plots of phase angle versus frequency.

NACA2-11 are 8.19 s, 1.42 s, 0.34 s, respectively. The decreased time constant of NACA2-11 compared with CA and ACA2 can be attributed to hierarchical porous structures and N-doping for more smooth accessibility of electrolyte ions, resulting in better rate performance than the other two samples.

To further study the practical performance of NACA2-11 electrode, two-electrode symmetrical supercapacitor is assembled and measured in 1 M H_2SO_4 (Fig. 6). The quasi-rectangular CV curves at scan rates from 10 to 200 mV s⁻¹ (Fig. 6a) and the nearly symmetric triangle GCD curves at high current densities (Fig. 6b) indicate good

EDL capacitive behavior and rate performance of the NACA2-11 electrode. As shown in Fig. 6c, the specific capacitance of NACA2-11 electrode is 228 F g^{-1} at 1 A g^{-1} , and still remains 120 F g^{-1} at a high current density of 50 A g^{-1} (53% of that at 1 A g^{-1}). The combination of good capacitance and rate performance of NACA2-11 is better than previously reported carbon-based electrodes (Fig. 6d and Table 2) [47–57]. Fig. 6e shows that NACA2-11 electrode exhibits a capacitive retention as high as 93% even after 10000 cycles at 5 A g^{-1} , and keeps a stable coulombic efficiency of 100%, demonstrating its good cycling stability. The symmetrical

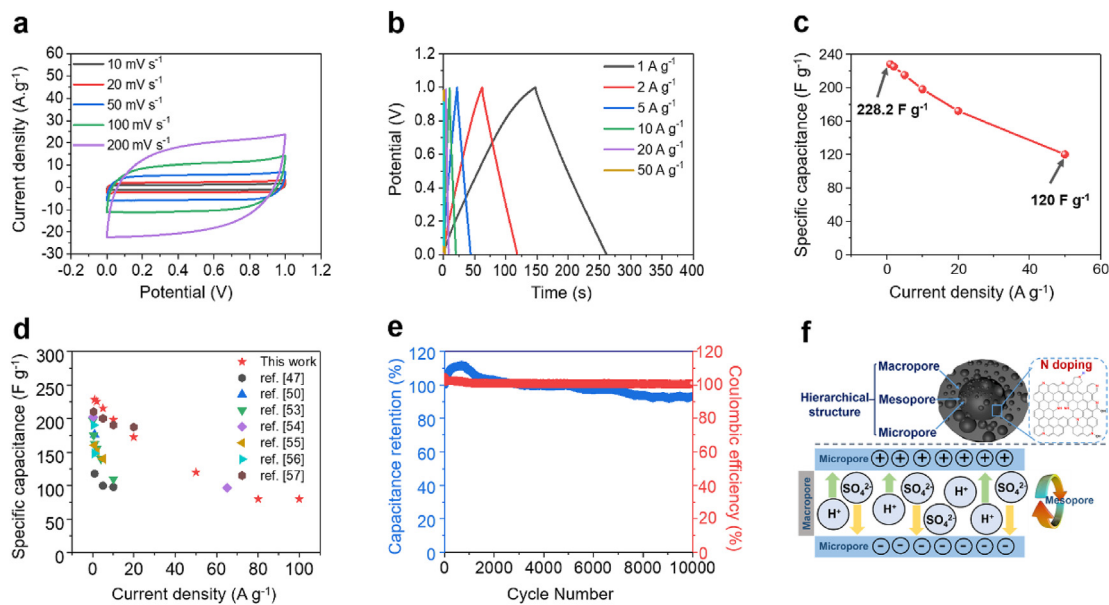


Fig. 6. Electrochemical performance of NACA2-11 measured with a two-electrode system in 1 M H_2SO_4 . (a) CV curves and (b) GCD curves. (c) The rate performance from 1 A g^{-1} to 50 A g^{-1} . (d) The comparison of specific capacitance with previously reported carbon electrodes. (e) The cycle performance. (f) Schematic illustration of electronic and ionic transport in NACA2-11 electrode.

Table 2

Comparison of electrochemical performance of porous carbon materials as electrode for supercapacitors.

Electrode	Surface area ($\text{m}^2 \text{ g}^{-1}$)	Electrolyte	Capacitance	Energy density	Power density	Rate	Cycle	Ref.
ANPC-3	1749	6 M KOH	243.2 $\text{F g}^{-1}/1 \text{ A g}^{-1}$	12.5 Wh kg^{-1}	450 W kg^{-1}	81.3%/ 10 A g^{-1}	96.5%/5000	[47]
N-YSHMCSs-2	1061	1 M H_2SO_4	169 $\text{F g}^{-1}/1 \text{ A g}^{-1}$	7.6 Wh kg^{-1}		70%/ 40 A g^{-1}	97.2%/5000	[48]
GO-160-8D	305	6 M KOH	436 $\text{F g}^{-1}/0.5 \text{ A g}^{-1}$			261 $\text{F g}^{-1}/50 \text{ A g}^{-1}$	94%/10000	[49]
NPGCs	1277	6 M KOH	261 $\text{F g}^{-1}/1 \text{ A g}^{-1}$	6.53 $\text{Wh kg}^{-1}/100 \text{ A g}^{-1}$	28.4 $\text{kW kg}^{-1}/100 \text{ A g}^{-1}$	189 $\text{F g}^{-1}/100 \text{ A g}^{-1}$	97%/20000	[50]
ACF@GR1	2035	6 M KOH	455.4 $\text{F g}^{-1}/1 \text{ A g}^{-1}$	12.2 $\text{Wh kg}^{-1}/20 \text{ A g}^{-1}$	4.7 $\text{kW kg}^{-1}/20 \text{ A g}^{-1}$	93.3 $\text{F g}^{-1}/20 \text{ A g}^{-1}$	90%/2000	[51]
NPC-GA-2	473	1 M H_2SO_4	608 $\text{F g}^{-1}/0.1 \text{ A g}^{-1}$	12.4 Wh kg^{-1}	2432 W kg^{-1}	250 $\text{F g}^{-1}/5 \text{ A g}^{-1}$	90%/10000	[52]
K800	2435.2	6 M KOH	197 $\text{F g}^{-1}/0.2 \text{ A g}^{-1}$	15 Wh kg^{-1}	20 kW kg^{-1}	108 $\text{F g}^{-1}/10 \text{ A g}^{-1}$	92.1%/10000	[53]
p-CNT/CGB	260	6 M KOH	202 $\text{F g}^{-1}/0.325 \text{ A g}^{-1}$	4.9 Wh kg^{-1}	150 Wh kg^{-1}	96.7 $\text{F g}^{-1}/65 \text{ A g}^{-1}$	97.4%/10000	[54]
N-CNT spherical particles		1 M H_2SO_4	215 $\text{F g}^{-1}/0.2 \text{ A g}^{-1}$			151 $\text{F g}^{-1}/5 \text{ A g}^{-1}$	99%/1500	[55]
NACA2-11	1410	1 M H_2SO_4	228 $\text{F g}^{-1}/1 \text{ A g}^{-1}$	15.8 Wh kg^{-1}	500 W kg^{-1}	120 $\text{F g}^{-1}/50 \text{ A g}^{-1}$	93%/10000	This work

supercapacitor based on NACA2-11 electrode exhibits a high energy density of 15.8 Wh kg^{-1} at a power density of 500 W kg^{-1} , which is much higher than that of commercial activated carbon ($\sim 5 \text{ Wh kg}^{-1}$) (Fig. S10). This superior capacitive performance of NACA2-11 electrode can be attributed to the synergistic effect of its hierarchical porous structures as well as heteroatom-doping, as schematically illustrated in Fig. 6f. In the hierarchical porous structure, micropores are beneficial for charge storing through forming electric double layers, which can dramatically promote the specific capacitance of carbon material. Nevertheless, since only micropores

(pore size $< 2 \text{ nm}$) go against the infiltration of electrolyte and transmission of ions, mesopores ($2 \text{ nm} < \text{pore size} < 50 \text{ nm}$) can accelerate the dynamic transport process avoiding invalid utilization of micropores, while macropores (pore size $> 50 \text{ nm}$) serve as the ion buffering reservoirs which can further shorten the ion transfer distance, leading to better rate performance. Moreover, N and O atoms in NACA2-11 can introduce pseudo-capacitance and improve the wettability of porous carbon material, resulting in higher capacitance and reduced solution resistance. The pseudo-capacitance contribution of NACA2-11 is estimated according to

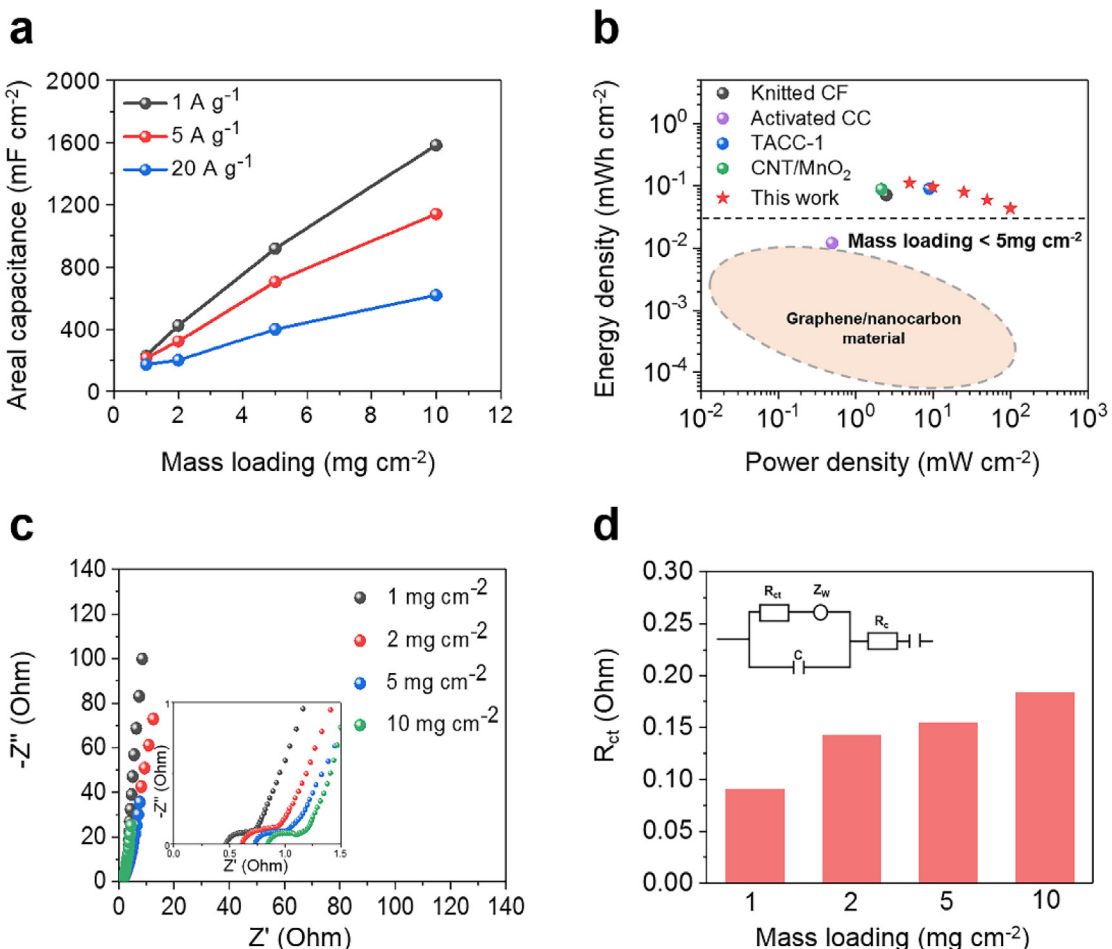


Fig. 7. Electrochemical performance of NACA2-11 measured with a two-electrode system in 1 M H_2SO_4 under different mass loadings. (a) Areal capacitance at different mass loadings and (b) Ragone plots at a mass loading of 10 mg cm^{-2} and comparison with previously reported carbon-based supercapacitors. (c) Nyquist plots. (d) Charge transfer resistance (R_{ct} , Ω) of the electrode with different mass loadings.

Dunn method in Fig. S11 and Fig. S12 [58]. The percentage of pseudo-capacitance varies from 33% to 3% when scan rate increases from 10 mV s^{-1} to 200 mV s^{-1} in the two-electrode system, indicating that the EDL capacitance become dominated with the increase of scan rates. Therefore, NACA2-11 with hierarchical porous structure and heteroatom-doping exhibits good charge storage capability and fast electrolyte ion transfer ability, leading to excellent capacitive performance especially at high charging densities.

A higher mass loading (at least 10 mg cm^{-2}) of electrode materials is essential for commercial utilizations. As shown in Fig. 7, the electrochemical performance of NACA2-11 is investigated at different areal mass loadings of 1, 2, 5 and 10 mg cm^{-2} , respectively. The gravimetric capacitance of the electrode shows a slight decrease with mass loading of active materials increasing from 1 to 10 mg cm^{-2} since electron/ion transport resistance would increase due to increased thickness (Fig. S13). Notably, the areal capacitance increases linearly with mass loading increasing from 1 to 10 mg cm^{-2} , indicating better capability for ionic diffusion and electron transport (Fig. 7a). The areal capacitance of NACA2-11 at the mass loading of 10 mg cm^{-2} reaches up to 1584 mF cm^{-2} at 1 A g^{-1} . The symmetric device based on NACA2-11//NACA2-11 with a high mass loading of 10 mg cm^{-2} exhibits a high areal energy density of 0.12 mWh cm^{-2} at a power density of 5 mW cm^{-2} , much better than those of previously reported electrode materials, such as carbon staple fiber yarn (knitted CF) ($0.071 \text{ mWh cm}^{-2}/2.5 \text{ mW cm}^{-2}$) [59], activated carbon cloth (activated CC) ($0.012 \text{ mWh cm}^{-2}/0.5 \text{ mW cm}^{-2}$) [60], thermally activated carbon (TACC-1) ($0.09 \text{ mWh cm}^{-2}/9 \text{ mW cm}^{-2}$) [61], carbon nanotubes/manganese dioxide (CNT/MnO₂) ($0.088 \text{ mWh cm}^{-2}/2.172 \text{ mW cm}^{-2}$) [62] (Fig. 7b). The excellent electrochemical performance is resulted from fast electron transport and ion diffusion of NACA2-11, as further reflected by the low electrochemical impedance in Fig. 7c and d. The charge transfer resistance (R_{ct}) of NACA2-11 only shows a slight increase with mass loading increasing. Moreover, the R_{ct} is only 0.18Ω when mass loading is elevated to 10 mg cm^{-2} , indicating that electron/ion transfer process is promoted due to the three-dimensional hierarchical porous structures in the thicker electrodes [63].

4. Conclusions

In summary, N-doping activated carbon aerogels have been prepared from polyimide gel with subsequent carbonization. The NACA exhibits a high surface area with multi-scale porous structures, in which micropores and mesopores can be easily controlled by tuning activating agent (KOH) and nitrogen sources (urea). Both micropore and mesopore volumes increase by increasing KOH amount, while the urea further increases the mesopore volume with the micropore volume remaining almost the same. Due to the synergistic effect of KOH and urea, NACA2-11 exhibits both high micropore (0.481 cc g^{-1}) and mesopore volume (0.566 cc g^{-1}), which respectively benefits the charge storage and ion diffusion as electrode materials for supercapacitors. In addition, the introduction of O and N atoms during KOH activation and carbonization with urea further increases the specific capacitance of NACA. Consequently, NACA2-11 exhibits a high capacitance of 228 F g^{-1} at 1 A g^{-1} in the two-electrode system, excellent rate capability with 53% retention at 50 A g^{-1} , and stays a good stability after 10000 cycles (93% retention). Furthermore, the practical device based on NACA2-11 electrode with a high mass loading of 10 mg cm^{-2} exhibits a high areal specific capacitance and low charge transfer resistance because of the fast ion diffusion kinetics. Therefore, the N-doping activated carbon aerogels thus prepared with a satisfying electrochemical performance will be promising materials for future studies in energy storage.

Notes

The authors declare no competing financial interest.

Acknowledgements

The authors are grateful for the financial support from the National Natural Science Foundation of China (21704014, 21674019), the Fundamental Research Funds for the Central Universities (2232017D-06, 2232019A3-03), Shanghai Sailing Program (17YF1400200), Program of Shanghai Academic Research Leader (17XD1400100), Shanghai Municipal Education Commission (17CG33), and Ministry of Education of the People's Republic of China (6141A0202202).

Appendix A. Supplementary data

Supplementary data to this article can be found online at <https://doi.org/10.1016/j.electacta.2019.134811>.

References

- [1] J. Yan, Q. Wang, T. Wei, Z. Fan, Recent advances in design and fabrication of electrochemical supercapacitors with high energy densities, *Adv. Energy Mater.* 4 (2014) 1300816.
- [2] Z. Li, W. Lv, C. Zhang, B. Li, F. Kang, Q. Yang, A sheet-like porous carbon for high-rate supercapacitors produced by the carbonization of an eggplant, *Carbon* 92 (2015) 11–14.
- [3] Y. Qing, Y. Jiang, H. Lin, L. Wang, A. Liu, Y. Cao, R. Sheng, Y. Guo, C. Fan, S. Zhang, D. Jia, Z. Fan, Boosting the supercapacitor performance of activated carbon by constructing overall conductive networks using graphene quantum dots, *J. Mater. Chem. A* 7 (2019) 6021–6027.
- [4] Y. Li, G. Wang, T. Wei, Z. Fan, P. Yan, Nitrogen and sulfur co-doped porous carbon nanosheets derived from willow catkin for supercapacitors, *Nano Energy* 19 (2016) 165–175.
- [5] Y. Miao, F. Li, H. Lu, J. Yan, Y. Huang, T. Liu, Nanocubic-Co₃O₄ coupled with nitrogen-doped carbon nanofiber network: a synergistic binder-free catalyst toward oxygen reduction reactions, *Compos. Commun.* 1 (2016) 15–19.
- [6] D. Zhai, B. Li, H. Du, G. Gao, L. Gan, Y. He, Q. Yang, F. Kang, The preparation of graphene decorated with manganese dioxide nanoparticles by electrostatic adsorption for use in supercapacitors, *Carbon* 50 (2012) 5034–5043.
- [7] J. Yan, J. Liu, Z. Fan, T. Wei, L. Zhang, High-performance supercapacitor electrodes based on highly corrugated graphene sheets, *Carbon* 50 (2012) 2179–2188.
- [8] J. Xu, Z. Tan, W. Zeng, G. Chen, S. Wu, Y. Zhao, K. Ni, Z. Tao, M. Ikram, H. Ji, Y. Zhu, A hierarchical carbon derived from sponge-templated activation of graphene oxide for high-performance supercapacitor electrodes, *Adv. Mater.* 28 (2016) 5222–5228.
- [9] F. Zhang, T. Liu, M. Li, M. Yu, Y. Luo, Y. Tong, Y. Li, Multiscale pore network boosts capacitance of carbon electrodes for ultrafast charging, *Nano Lett.* 17 (2017) 3097–3104.
- [10] M. Vijaykumar, D.S. Rohita, T.N. Rao, M. Karthik, Electrode mass ratio impact on electrochemical capacitor performance, *Electrochim. Acta* 298 (2019) 347–359.
- [11] Z. Pan, H. Zhi, Y. Qiu, J. Yang, L. Xing, Q. Zhang, X. Ding, X. Wang, G. Xu, H. Yuan, M. Chen, W. Li, Y. Yao, N. Motta, M. Liu, Y. Zhang, Achieving commercial-level mass loading in ternary-doped holey graphene hydrogel electrodes for ultrahigh energy density supercapacitors, *Nano Energy* 46 (2018) 266–276.
- [12] N. Mao, H. Wang, Y. Sui, Y. Cui, J. Pokrzywinski, J. Shi, W. Liu, S. Chen, X. Wang, D. Mitlin, Extremely high-rate aqueous supercapacitor fabricated using doped carbon nanoflakes with large surface area and mesopores at near-commercial mass loading, *Nano Res* 10 (2017) 1767–1783.
- [13] W. Fan, Y. Xia, W.W. Tjiu, P.K. Pallathadka, C. He, T. Liu, Nitrogen-doped graphene hollow nanospheres as novel electrode materials for supercapacitor applications, *J. Power Sources* 243 (2013) 973–981.
- [14] W. Zhang, C. Xu, C. Ma, G. Li, Y. Wang, K. Zhang, F. Li, C. Liu, H. Cheng, Y. Du, N. Tang, W. Ren, Nitrogen-superdoped 3D graphene networks for high-performance supercapacitors, *Adv. Mater.* 29 (2017), 1701677.
- [15] F. Zhang, T. Liu, J. Zhang, E. Cui, L. Yue, R. Jiang, G. Hou, The potassium hydroxide-urea synergy in improving the capacitive energy-storage performance of agar-derived carbon aerogels, *Carbon* 147 (2019) 451–459.
- [16] Z. Song, W. Li, Y. Bao, Z. Sun, L. Gao, M.H. Nawaz, D. Han, L. Niu, A new route to tailor high mass loading all-solid-state supercapacitor with ultra-high volumetric energy density, *Carbon* 136 (2018) 46–53.
- [17] H. Ma, Q. Zhou, M. Wu, M. Zhang, B. Yao, T. Gao, H. Wang, C. Li, D. Sui, Y. Chen, G. Shi, Tailoring the oxygenated groups of graphene hydrogels for high-performance supercapacitors with large areal mass loadings, *J. Mater. Chem.*

- A 6 (2018) 6587–6594.
- [18] L. Sheng, J. Chang, L. Jiang, Z. Jiang, Z. Liu, T. Wei, Z. Fan, Multilayer-folded graphene ribbon film with ultrahigh areal capacitance and high rate performance for compressible supercapacitors, *Adv. Funct. Mater.* 28 (2018) 1800597.
- [19] Z. Fan, Q. Zhao, T. Li, J. Yan, Y. Ren, J. Feng, T. Wei, Easy synthesis of porous graphene nanosheets and their use in supercapacitors, *Carbon* 50 (2012) 1699–1703.
- [20] Q. Wang, J. Yan, Y. Wang, T. Wei, M. Zhang, X. Jing, Z. Fan, Three-dimensional flower-like and hierarchical porous carbon materials as high-rate performance electrodes for supercapacitors, *Carbon* 67 (2014) 119–127.
- [21] S. Liu, L. Ge, S. Gao, L. Zhuang, Z. Zhu, H. Wang, Activated carbon derived from bio-waste hemp hurd and retted hemp hurd for CO₂ adsorption, *Compos. Commun.* 5 (2017) 27–30.
- [22] S. Zuo, J. Chen, W. Liu, X. Li, Y. Kong, C. Yao, Y. Fu, Preparation of 3D interconnected hierarchical porous N-doped carbon nanotubes, *Carbon* 129 (2018) 199–206.
- [23] L. Yao, Q. Wu, P. Zhang, J. Zhang, D. Wang, Y. Li, X. Ren, H. Mi, L. Deng, Z. Zheng, Scalable 2D hierarchical porous carbon nanosheets for flexible supercapacitors with ultrahigh energy density, *Adv. Mater.* 30 (2018) 1706054.
- [24] J. Zhao, H. Lai, Z. Lyu, Y. Jiang, K. Xie, X. Wang, Q. Wu, L. Yang, Z. Jin, Y. Ma, J. Liu, Z. Hu, Hydrophilic hierarchical nitrogen-doped carbon nanocages for ultrahigh supercapacitive performance, *Adv. Mater.* 27 (2015) 3541–3545.
- [25] Y. Zhang, W. Fan, H. Lu, T. Liu, Highly porous polyimide-derived carbon aerogel as advanced three-dimensional framework of electrode materials for high-performance supercapacitors, *Electrochim. Acta* 283 (2018) 1763–1772.
- [26] F. Li, L. Xie, G. Sun, Q. Kong, F. Su, Y. Cao, J. Wei, A. Ahmad, X. Guo, C. Chen, Resorcinol-formaldehyde based carbon aerogel: preparation, structure and applications in energy storage devices, *Microporous Mesoporous Mater.* 279 (2019) 293–315.
- [27] M. Li, C. Liu, H. Cao, H. Zhao, Y. Zhang, Z. Fan, KOH self-templating synthesis of three-dimensional hierarchical porous carbon materials for high performance supercapacitors, *J. Mater. Chem. A* 2 (2014) 14844.
- [28] S. Yu, Y. Li, N. Pan, KOH activated carbon/graphene nanosheets composites as high performance electrode materials in supercapacitors, *RSC Adv.* 4 (2014) 48758–48764.
- [29] X. Zhang, H. Zhang, C. Li, K. Wang, X. Sun, Y. Ma, Recent advances in porous graphene materials for supercapacitor applications, *RSC Adv.* 4 (2014) 45862–45884.
- [30] E.J. Lee, Y.J. Lee, J.K. Kim, M. Lee, J. Yi, J.R. Yoon, J.C. Song, I.K. Song, Oxygen group-containing activated carbon aerogel as an electrode material for supercapacitor, *Mater. Res. Bull.* 70 (2015) 209–214.
- [31] X. Tang, C. Liu, X. Chen, Y. Deng, X. Chen, J. Shao, Q. Yang, Graphene aerogel derived by purification-free graphite oxide for high performance supercapacitor electrodes, *Carbon* 146 (2019) 147–154.
- [32] X. Wu, D. Yang, C. Wang, Y. Jiang, T. Wei, Z. Fan, Functionalized three-dimensional graphene networks for high performance supercapacitors, *Carbon* 92 (2015) 26–30.
- [33] M.C. Gutiérrez, F. Picó, F. Rubio, J. Manuel Amarilla, F. Javier Palomares, M.L. Ferrer, F. Del Monte, J.M. Rojo, PPO₁₅-PEO₂₂-PPO₁₅ block copolymer assisted synthesis of monolithic macro- and microporous carbon aerogels exhibiting high conductivity and remarkable capacitance, *J. Mater. Chem.* 19 (2009) 1236.
- [34] R. Liu, L. Pan, X. Liu, D. Wu, An evaporation-induced tri-constituent assembly approach to fabricate an ordered mesoporous carbon/graphene aerogel for high-performance supercapacitors, *RSC Adv.* 5 (2015) 16765–16768.
- [35] M. Li, C. Liu, H. Cao, H. Zhao, Y. Zhang, Z. Fan, KOH self-templating synthesis of three-dimensional hierarchical porous carbon materials for high performance supercapacitors, *J. Mater. Chem. A* 2 (2014) 14844.
- [36] C. Tang, Y. Liu, D. Yang, M. Yang, H. Li, Oxygen and nitrogen co-doped porous carbons with finely-layered schistose structure for high-rate-performance supercapacitors, *Carbon* 122 (2017) 538–546.
- [37] Q. Wang, Y. Lei, Y. Zhu, H. Wang, J. Feng, G. Ma, Y. Wang, Y. Li, B. Nan, Q. Feng, Z. Lu, H. Yu, Edge defect engineering of nitrogen-doped carbon for oxygen electrocatalysts in Zn–Air Batteries, *ACS Appl. Mater. Interfaces* 10 (2018) 29448–29456.
- [38] M. Majumder, R.B. Choudhary, A.K. Thakur, Hemispherical nitrogen-doped carbon spheres integrated with polyindole as high performance electrode material for supercapacitor applications, *Carbon* 142 (2019) 650–661.
- [39] Q. Shi, R. Zhang, Y. Lv, Y. Deng, A.A. Elzatahrya, D. Zhao, Nitrogen-doped ordered mesoporous carbons based on cyanamide as the dopant for supercapacitor, *Carbon* 84 (2015) 335–346.
- [40] S. Zuo, J. Chen, W. Liu, X. Li, Y. Kong, C. Yao, Y. Fu, Preparation of 3D interconnected hierarchical porous N-doped carbon nanotubes, *Carbon* 129 (2018) 199–206.
- [41] D. Lee, M. Jin, D. Oh, S. Lee, J. Park, Straightforward synthesis of hierarchically porous nitrogen-doped carbon via pyrolysis of chitosan/urea/KOH mixtures and its application as a support for formic acid dehydrogenation catalysts, *ACS Sustain. Chem. Eng.* 5 (2017) 9935–9944.
- [42] J. Duch, P. Kubisaik, K.H. Adolfsson, M. Hakkarainen, M. Golda-Cepa, A. Kotarba, Work function modifications of graphite surface via oxygen plasma treatment, *Appl. Surf. Sci.* 419 (2017) 439–446.
- [43] H. Chen, J. Chen, D. Chen, H. We, P. Liu, W. Wei, Nitrogen- and oxygen-rich dual-decorated carbon materials with porosity for high-performance supercapacitors, *J. Mater. Sci.* 54 (2019) 5625–5640.
- [44] H. Cheng, X. Zhou, A. Gao, F. Yi, D. Shu, X. Song, Supermolecule polymerization derived porous nitrogen-doped reduced graphene oxide as a high-performance electrode material for supercapacitors, *Electrochim. Acta* 292 (2018) 20–30.
- [45] L. Ni, R. Wang, H. Wang, C. Sun, B. Sun, X. Guo, Designing nanographitic domains in N-doped porous carbon foam for high performance supercapacitors, *Carbon* 139 (2018) 1152–1159.
- [46] Z. Liu, K. Xiao, H. Guo, X. Ning, A. Hu, Q. Tang, B. Fan, Y. Zhu, X. Chen, Nitrogen-doped worm-like graphitized hierarchical porous carbon designed for enhancing area-normalized capacitance of electrical double layer supercapacitors, *Carbon* 117 (2017) 163–173.
- [47] G. Lin, R. Ma, Y. Zhou, Q. Liu, X. Dong, J. Wang, KOH activation of biomass-derived nitrogen-doped carbons for supercapacitor and electrocatalytic oxygen reduction, *Electrochim. Acta* 261 (2018) 49–57.
- [48] C. Liu, J. Wang, J. Li, M. Zeng, R. Luo, J. Shen, X. Sun, W. Han, L. Wang, Synthesis of N-doped hollow-structured mesoporous carbon nanospheres for high-performance supercapacitors, *ACS Appl. Mater. Interfaces* 8 (2016) 7194–7204.
- [49] Z. Liu, L. Jiang, L. Sheng, Q. Zhou, T. Wei, B. Zhang, Z. Fan, Oxygen clusters distributed in graphene with “Paddy Land” structure: ultrahigh capacitance and rate performance for supercapacitors, *Adv. Funct. Mater.* 28 (2018), 1705258.
- [50] W. Yang, L. Hou, X. Xu, Z. Li, X. Ma, F. Yang, Y. Li, Carbon nitride template-directed fabrication of nitrogen-rich porous graphene-like carbon for high performance supercapacitors, *Carbon* 130 (2018) 325–332.
- [51] Q. Xie, R. Bao, C. Xie, A. Zheng, S. Wu, Y. Zhang, R. Zhang, P. Zhao, Core-shell N-doped active carbon fiber@graphene composites for aqueous symmetric supercapacitors with high-energy and high-power density, *J. Power Sources* 317 (2016) 133–142.
- [52] C. Wang, Y. Huang, H. Pan, J. Jiang, X. Yang, Z. Xu, H. Tian, S. Han, D. Wu, Nitrogen-doped porous carbon/graphene aerogel with much enhanced capacitive behaviors, *Electrochim. Acta* 215 (2016) 100–107.
- [53] P. Hao, Z. Zhao, Y. Leng, J. Tian, Y. Sang, R.I. Boughton, C.P. Wong, H. Liu, B. Yang, Graphene-based nitrogen self-doped hierarchical porous carbon aerogels derived from chitosan for high performance supercapacitors, *Nano Energy* 15 (2015) 9–23.
- [54] B.S. Mao, Z. Wen, Z. Bo, J. Chang, X. Huang, J. Chen, Hierarchical nano-hybrids with porous CNT-networks decorated crumpled graphene balls for supercapacitors, *ACS Appl. Mater. Interfaces* 6 (2014) 9881–9889.
- [55] D. Gueon, J.H. Moon, Nitrogen-doped carbon nanotube spherical particles for supercapacitor applications: emulsion-assisted compact packing and capacitance enhancement, *ACS Appl. Mater. Interfaces* 7 (2015) 20083–20089.
- [56] S. Zheng, H. Ju, X. Lu, A high-performance supercapacitor based on KOH activated 1D C₇₀ microstructures, *Adv. Energy Mater.* 5 (2015), 1500871.
- [57] H. Kim, A.R. Kamali, K.C. Roh, K. Kim, D.J. Fray, Dual coexisting interconnected graphene nanostructures for high performance supercapacitor applications, *Energy Environ. Sci.* 9 (2016) 2249–2256.
- [58] M. Forghani, S.W. Donne, Complications when differentiating charge transfer processes in electrochemical capacitor materials: assessment of cyclic voltammetry data, *J. Electrochem. Soc.* 8 (2019) 1370–1379.
- [59] K. Jost, D. Stenger, C. Perez, J. McDonough, K. Lian, Y. Gogotsi, G. Dion, Knitted and screen printed carbon-fiber supercapacitors for applications in wearable electronics, *Energy Environ. Sci.* 6 (2013) 2698–2705.
- [60] G. Wang, H. Wang, X. Lu, Y. Ling, M. Yu, T. Zhai, Y. Tong, Y. Li, Solid-state supercapacitor based on activated carbon cloths exhibits excellent rate capability, *Adv. Mater.* 26 (2014) 2676–2682.
- [61] Q. Wang, W. Ren, F. Gao, C. Qiu, Q. Wang, F. Gao, C. Zhao, Thermally activated multilayered carbon cloth as flexible supercapacitor electrode material with significantly enhanced areal energy density, *ChemElectroChem* 6 (2019) 1768–1775.
- [62] L. Dong, C. Xu, Y. Li, Z. Pan, G. Liang, E. Zhou, F. Kang, Q. Yang, Breathable and wearable energy storage based on highly flexible paper electrodes, *Adv. Mater.* 28 (2016) 9313–9319.
- [63] Z. Li, X. Liu, L. Wang, F. Bu, J. Wei, D. Pan, M. Wu, Hierarchical 3D all-carbon composite structure modified with N-doped graphene quantum dots for high-performance flexible supercapacitors, *Small* 14 (2018) 1801498.